PNAS RESEARCH ARTICLE | MEDICAL SCIENCES

Calcium channel blockers potentiate gemcitabine chemotherapy in pancreatic cancer

Daniel R. Principe[a,b,c], Alexandre F. Aissa[c], Sandeep Kumar[b], Thao N. D. Pham[d], Patrick W. Underwood[e], Rakesh Nair[b], Rong Ke[b], Basabi Rana[b], Jose G. Trevino[f], Hidayatullah G. Munshi[d,g], Elizaveta V. Benevolenskaya[c,1], and Ajay Rana[b,g,1]

Edited by Arul Chinnaiyan, University of Michigan Medical School, Ann Arbor, MI; received January 4, 2022; accepted March 19, 2022

There is currently no effective treatment for pancreatic ductal adenocarcinoma (PDAC). While palliative chemotherapy offers a survival benefit to most patients, nearly all will eventually progress on treatment and long-term survivability remains poor. Given the lack of subsequent line treatment options, in this study, we sought to identify novel strategies to prevent, delay, or overcome resistance to gemcitabine, one of the most widely used medications in PDAC. Using a combination of single-cell RNA sequencing and high-throughput proteomic analysis, we identified a subset of gemcitabine-resistant tumor cells enriched for calcium/calmodulin signaling. Pharmacologic inhibition of calcium-dependent calmodulin activation led to the rapid loss of drug-resistant phenotypes in vitro, which additional single-cell RNA sequencing identified was due to impaired activation of the RAS/ERK signaling pathway. Consistent with these observations, calcium chelation or depletion of calcium in the culture media also impaired ERK activation in gemcitabine-resistant cells, and restored therapeutic responses to gemcitabine in vitro. We observed similar results using calcium channel blockers (CCBs) such as amlodipine, which inhibited prosurvival ERK signaling in vitro and markedly enhanced therapeutic responses to gemcitabine in both orthotopic xenografts and transgenic models of PDAC. Combined, these results offer insight into a potential means of gemcitabine resistance and suggest that select CCBs may provide a clinical benefit to PDAC patients receiving gemcitabine-based chemotherapy.

pancreatic cancer | chemotherapy | gemcitabine | drug resistance

Pancreatic ductal adenocarcinoma (PDAC) often presents at late clinical stages and is associated with poor outcomes and significant disease morbidity. While surgical resection offers the most significant survival benefit, most patients are diagnosed with metastatic disease and are ineligible for surgery (1). Regardless of whether surgery is performed, nearly all intent-to-treat patients will receive broad-spectrum chemotherapy. In the first-line setting, most patients are offered the multidrug regimen FOLFIRINOX (5-fluorouracil, leucovorin, irinotecan, and oxaliplatin) or gemcitabine with albumin-conjugated (nab)-paclitaxel. Following progressive disease on FOLFIRINOX, the combination of gemcitabine and nab-paclitaxel can be offered as a second-line treatment (2). Though the combination of 5-fluorouracil, leucovorin, and liposomal irinotecan is approved following progression on gemcitabine-based chemotherapy, this approach only modestly extends survival (3). Hence, gemcitabine resistance remains a pressing issue in clinical oncology, and there is an immediate need for new therapeutic approaches to either enhance the efficacy of gemcitabine-based chemotherapy or restore drug sensitivity for patients with gemcitabine-refractory PDAC.

While several molecular mechanisms for gemcitabine resistance have been suggested, these have yet to translate to a safe and effective strategy to potentiate the effects of chemotherapy in the clinic. For example, the receptor tyrosine kinase epidermal growth factor receptor (EGFR) has been linked to gemcitabine resistance in preclinical studies (4). However, the combination of gemcitabine and the selective EGFR inhibitor erlotinib has since been evaluated in a large-scale phase III trial, improving median overall survival by less than 2 wk compared with gemcitabine alone (5). Gemcitabine has been combined with several other targeted therapies in clinical trials, including drugs targeting EGFR (5), Smoothened (6), and vascular endothelial growth factor (7, 8). Despite the clear link between each of these molecules and gemcitabine resistance in preclinical studies (9–11), the results of these trials have largely been negative, with little change in overall or progression-free survival (5–8). As a result, erlotinib remains the only Food and Drug Administration (FDA)–approved targeted therapy for use in combination with gemcitabine, though its long-term benefit is unclear (12).

In the present study, we sought to provide additional insight into gemcitabine resistance in PDAC, with the goal of identifying a more effective strategy to improve drug

Significance

Pancreatic cancer is a leading cause of cancer-related death, in part due to incomplete responses to standard-of-care chemotherapy. In this study, using a combination of single-cell RNA sequencing and high-throughput proteomics, we identified the calcium-responsive protein calmodulin as a key mediator of resistance to the first-line chemotherapy agent gemcitabine. Inhibition of calmodulin led to the loss of gemcitabine resistance in vitro, which was recapitulated using a calcium chelator or Food and Drug Administration–approved calcium channel blockers (CCBs), including amlodipine. In animal studies, amlodipine markedly enhanced therapeutic responses to gemcitabine chemotherapy, reducing the incidence of distant metastases and extending survival. Hence, incorporating CCBs may provide a safe and effective means of improving responses to gemcitabine-based chemotherapy in pancreatic cancer patients.

Author contributions: D.R.P., S.K., and A.R. designed research; D.R.P., A.F.A., S.K., T.N.D.P., R.N., R.K., and E.V.B. performed research; A.F.A., T.N.D.P., P.W.U., B.R., J.G.T., H.G.M., E.V.B., and A.R. contributed new reagents/analytic tools; and D.R.P. and A.R. wrote the paper.

The authors declare no competing interest.

This article is a PNAS Direct Submission.

[1]To whom correspondence may be addressed. Email: arana@uic.edu or evb@uic.edu.

This article contains supporting information online at http://www.pnas.org/lookup/suppl/doi:10.1073/pnas.2200143119/-/DCSupplemental.

Published April 27, 2022.

responses in the clinic. We first challenged an established PDAC cell line with a tolerable dose of gemcitabine and conducted single-cell RNA sequencing. This revealed unique, drug-resistant populations enriched for calcium ion binding and calmodulin/NFAT signaling pathways. When resistant clones were selected by incubating cells with increasing concentrations of gemcitabine for several passages, whole-proteome analysis revealed a significant up-regulation of calmodulin 2 (CALM2), consistent with our prior sequencing data. Pharmacologic inhibition of calcium-dependent calmodulin activation restored gemcitabine sensitivity in vitro, which further single-cell RNA-sequencing analysis revealed was associated with the inhibition of prosurvival ERK signaling, a known driver of gemcitabine resistance (13–16). This was recapitulated using the calcium chelator BAPTA-AM, which similarly mitigated ERK activation and restored gemcitabine sensitivity in vitro.

Based on retrospective clinical data that PDAC patients receiving the L-type calcium channel (LTCC) inhibitor amlodipine may have improved clinical outcomes when administered gemcitabine-based chemotherapy (17), we hypothesized that LTCC inhibition might be an effective means of depleting intracellular calcium, thereby disrupting calmodulin-dependent ERK pathway activation. Accordingly, incubation with the calcium channel blockers (CCBs) amlodipine or nifedipine restored gemcitabine sensitivity in vitro, also attributed to the inhibition of ERK signaling. Amlodipine similarly reduced ERK activation in ex vivo slice cultures of PDAC tumors and restored gemcitabine sensitivity in orthotopic xenografts of gemcitabine-resistant (GR) tumor cells, reducing metastases and extending overall survival. Finally, amlodipine enhanced the antineoplastic effects of gemcitabine in an aggressive model of transgenic PDAC, markedly improving survival compared with gemcitabine monotherapy. Combined, these results suggest that calcium-dependent calmodulin activation may function as a potential means of gemcitabine escape in PDAC. Based on these observations, CCBs such as amlodipine warrant additional exploration as an adjuvant to gemcitabine-based chemotherapy, particularly given their low cost and favorable toxicity profiles.

Results

Select GR Tumor Cells Are Enriched for Calmodulin/NFAT Signaling. Recent evidence suggests that, like human tumors, cancer cell lines can be highly heterogeneous in culture (18). Therefore, we sought to explore the innate heterogeneity of the widely used PANC-1 cell line and identify potential subpopulations that demonstrate intrinsic resistance to gemcitabine-induced cell death. We first conducted a short-term experiment comparing untreated and gemcitabine-treated PANC-1 cells after 24 h, the point at which drug-treated cells begin to show early signs of stress, growth arrest, and/or death. Cells were serum-starved overnight, and then changed to full-serum media containing 1 μM gemcitabine for 24 h. Cells were then collected, subjected to single-cell RNA sequencing, and compared with untreated PANC-1 cells. Following sequencing, cell populations were visualized via Seurat's uniform manifold approximation and projection (UMAP) dimensionality reduction. Gemcitabine-treated PANC-1 cells were transcriptionally distinct from the untreated population (Fig. 1*A*). Using the previously described criteria (19), cells were clustered based on transcriptional similarity. When visualized, untreated PANC-1 cells and gemcitabine-treated cells were each represented by three nonoverlapping clusters (Fig. 1*B*). Following clustering, cell-cycle genes were evaluated to determine the cell-cycle phase positioning of each cell population (Fig. 1*C*). Select hierarchical genes used to determine cell clustering are shown in Fig. 1*D*.

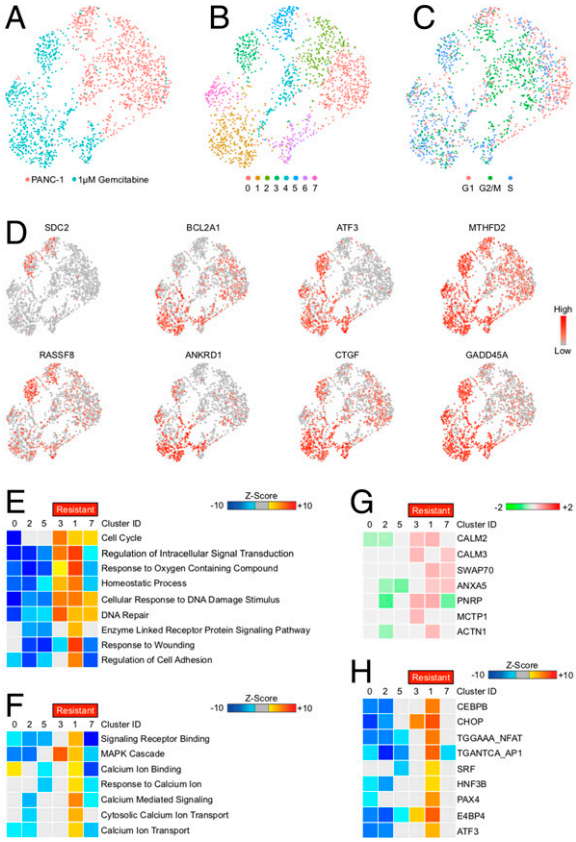

Fig. 1. Select GR tumor cells are enriched for calmodulin/NFAT signaling. (*A*) PANC-1 tumor cells were incubated with either a saline vehicle or 1 μM gemcitabine and analyzed by single-cell RNA sequencing as described, and populations were visualized via UMAP scatterplot. (*B*) Control and drug-treated PANC-1 cells were grouped into eight transcriptionally distinct clusters (see also *SI Appendix*, Fig. S1*A*). (*C*) Each cell was analyzed for cell cycle–related genes, and the stage of the cell cycle is shown, with GR clusters demonstrating increased expression of S phase genes. (*D*) Select genes used in the cell-clustering algorithm. (*E*) Functional enrichment analysis for GO biological process terms using GiTools statistics. Top GO terms exhibiting differences in gemcitabine-treated clusters (resistant) compared with untreated clusters and displaying >15 genes per term are shown. (*F*) Enrichment analysis for GO terms related to cell signaling. (*G*) Individual genes significantly up-regulated in the calcium ion binding gene set in GR clusters. (*H*) Transcriptional enrichment of known NFAT targets in each cell cluster.

Based on the expression of S phase genes and lack of genes involved in cell stress/cell death, gemcitabine-associated clusters 3, 1, and 7 were presumed as potentially GR. To gain insight into the potential signaling pathways driving these more drug-resistant phenotypes, we next conducted enrichment analysis for genes in relation to Gene Ontology (GO) biological processes in each cluster (Fig. 1*E*). The GR clusters displayed significant up-regulation of several cell processes, namely genes involved in the cell cycle, accommodating cell stress and DNA damage (Fig. 1*E*). Additionally, the hyperresistant cluster 1 also displayed significant up-regulation of more focused gene sets, namely receptor ligand binding, mitogen-activated protein kinase (MAPK) signaling, and several gene sets involved in calcium ion transport, binding, and signaling (Fig. 1*F*). Specifically, drug-resistant clusters displayed up-regulation in several genes associated with intracellular calcium signal transduction, namely CALM2, that was most strongly up-regulated in cluster 1 (Fig. 1*G*). As calmodulin is known to exert its effect in part

through the downstream activation of NFAT, we next determined the relative expression of known NFAT targets. Consistent with enhanced CALM2 expression, cluster 1 displayed significant enrichment for NFAT target genes, while NFAT genes were among genes with decreased expression in clusters of untreated cells (Fig. 1*H*).

Calmodulin Is Frequently Overexpressed in Gemcitabine-Treated PDAC. To generate a more uniformly GR model system, we again used the PANC-1 cell line, and generated drug-resistant populations by culturing cells in increasing concentrations of gemcitabine for several passages until viable in concentrations well beyond the IC_{50} (Fig. 2*A*). Once these GR populations were established (Fig. 2*B*), the drug-resistant phenotype was confirmed by 3-(4,5-Dimethylthiazol-2-yl)-2,5-diphenyltetrazolium bromide (MTT) assay using increasing concentrations of gemcitabine, which showed an expected decline in viability for naïve PANC-1 cells yet no significant change in cell viability in PANC-1-GR cells (Fig. 2*C*). Similar results were observed in cell death, as concentrations of 5 and 10 μM led to a strong apoptotic response in naïve cells, with little to no apoptosis observed in GR cells (Fig. 2 *D* and *E*).

After verifying the GR phenotype, we next compared the proteome of PANC-1 and PANC-1-GR cells using two-dimensional (2D) gel electrophoresis (*SI Appendix*, Fig. S1*A*). This revealed several differentially expressed proteins between the two cell lines, including serine and arginine–rich splicing factor 3 (SRSF3), the ALEX family member ARMX1, keratin, type II cytoskeletal 1 (K2C1), and others (*SI Appendix*, Fig. S1*B*). However, consistent with previous single-cell RNA-sequencing data, PANC-1-GR cells also had a nearly fourfold increase in the expression of CALM2 (Fig. 2 *F* and *G*), similar to the intrinsically drug-resistant and CALM2-enriched population identified in Fig. 1. After confirming this increase by Western blot (Fig. 2*H*), we evaluated calmodulin expression in 36 PDAC surgical specimens. Of these 36 patients, 18 were chemotherapy-naïve and 18 received neoadjuvant gemcitabine-based chemotherapy before surgery. Consistent with our in vitro data, gemcitabine-treated patient specimens generally had more robust calmodulin expression than chemotherapy-naïve patients, localizing predominantly to the cytoplasm and cell membrane of the neoplastic epithelium (Fig. 2*I*).

As this could potentially be confounded through disease heterogeneity, we next evaluated this phenomenon using two established models of murine PDAC. The first was the well-established Pdx1-Cre × LSL-*Kras*^{G12D} × LSL-*TP53*^{R172H} (KPC) model of invasive PDAC. This model faithfully recapitulates human PDAC histotypes with several key features, including poor responses to chemotherapy. To model the long-term effects of gemcitabine, mice were allowed to develop overt PDAC for a minimum of 3.5 mo, at which point they were randomized at a 50:50 male-to-female ratio into one of two treatment groups ($n = 4$ per group). Mice were treated with intraperitoneal (IP) injections of either phosphate-buffered saline (PBS) vehicle or 100 mg/kg gemcitabine twice per week and killed when showing clear signs of health decline, for example weight loss, ascites, or lethargy (Fig. 2*J*; $n = 4$ or 5 per group).

In parallel experiments, we also used the G-68 cell line–derived xenograft (CDX), as described in our previous publication (20). This model uses a primary pancreatic cancer cell line derived from a non-Hispanic, white female with a T3N1 tumor harboring KRAS^{G12D} and TP53^{R248W} mutations similar to those used in the KPC model. Cells (5×10^6) were subsequently injected into the flank of NOD scid gamma (NSG) mice and, once tumors reached 100 to 200 mm^3 in size, animals were treated with either vehicle or 40 mg/kg of gemcitabine once per week (Fig. 2*K*; $n = 4$ or 5 per group). In both KPC and G-68 mouse models, gemcitabine-treated animals consistently had uniform up-regulation of calmodulin by immunohistochemistry, often localizing to the cell membrane (Fig. 2*L*).

Given the inherent limitations of 2D cell culture and the animal models described above, we next established ex vivo slice cultures of two PDAC patients undergoing surgical resection by sectioning a 6-mm tumor core at 250-μm intervals and culturing as described (21, 22). After sectioning, slice cultures were incubated with either a PBS vehicle or 5 μM gemcitabine and evaluated after 72 h by immunohistochemistry (Fig. 2*M*). Consistent with our previous observations, slice cultures treated with gemcitabine had increased staining for calmodulin, which localized predominantly to the neoplastic epithelium (Fig. 2*N*).

Calmodulin-Dependent ERK Activation Is Required for Gemcitabine Resistance In Vitro. To determine the biologic significance of calmodulin signaling in gemcitabine resistance, we next conducted a series of cell-viability assays using PANC-1-GR cells, treating cells with increasing concentrations of gemcitabine with or without inhibitors of canonical calmodulin signaling. PANC-1-GR cells were serum-starved overnight, and pretreated with a dimethyl sulfoxide (DMSO) control (1:1,000), an NFAT-inhibiting peptide (NFATi) (25 μM), the CAMK inhibitor KN-62 (10 μM), or the cell-permeable antagonist of calcium-dependent calmodulin activation W-7 (10 μM). At this time, cells were changed to full-serum media with additional inhibitors, as well as varying doses of gemcitabine. After another 48 h, cell viability was evaluated by MTT assay. Though W-7–mediated calmodulin inhibition led to the loss of the GR phenotype, reducing cell viability and increasing drug-induced apoptosis, there was no effect on cell viability using either KN-62 or NFATi (Fig. 3 *A*–*C*).

Thus, as the canonical targets of calmodulin signals do not appear to have a role in the maintenance of gemcitabine resistance, we next treated PANC-1-GR with W-7 as described and, after 24 h, conducted single-cell RNA sequencing. Cells were then displayed via UMAP dimensionality reduction, and clustered as previously. Using this approach, untreated and W-7–treated cells were each represented by five clusters (Fig. 3 *D* and *E*). We again conducted enrichment analysis for genes in relation to GO biological processes in each cluster, revealing a significant down-regulation in several cell processes, most notably those involved in the cell cycle (Fig. 3*F*). As these cell-cycle genes could potentially have a disproportionate impact on clustering, we next excluded cell-cycle genes from analysis and re-formed cell clusters (*SI Appendix*, Fig. S2*A*). Untreated PANC-1-GR cells were represented by six well-defined clusters and treated cells were represented by five, with little overlap between groups (*SI Appendix*, Fig. S2*B*). Moreover, treated cells still displayed a highly significant reduction in the same cell processes compared with untreated cells (*SI Appendix*, Fig. S2*C*).

To determine a potential mechanism to explain these findings, we conducted subsequent gene set enrichment analysis in each cluster for known cell signaling pathways. This revealed significant W-7–mediated suppression of GO signal receptor binding pathways, as well as genes in the GO MAPK and ERK1/2 cascade gene sets (Fig. 3 *G*–*I*). We therefore explored the biologic significance of ERK inhibition with respect to the GR phenotype by repeating cell-viability assays as described,

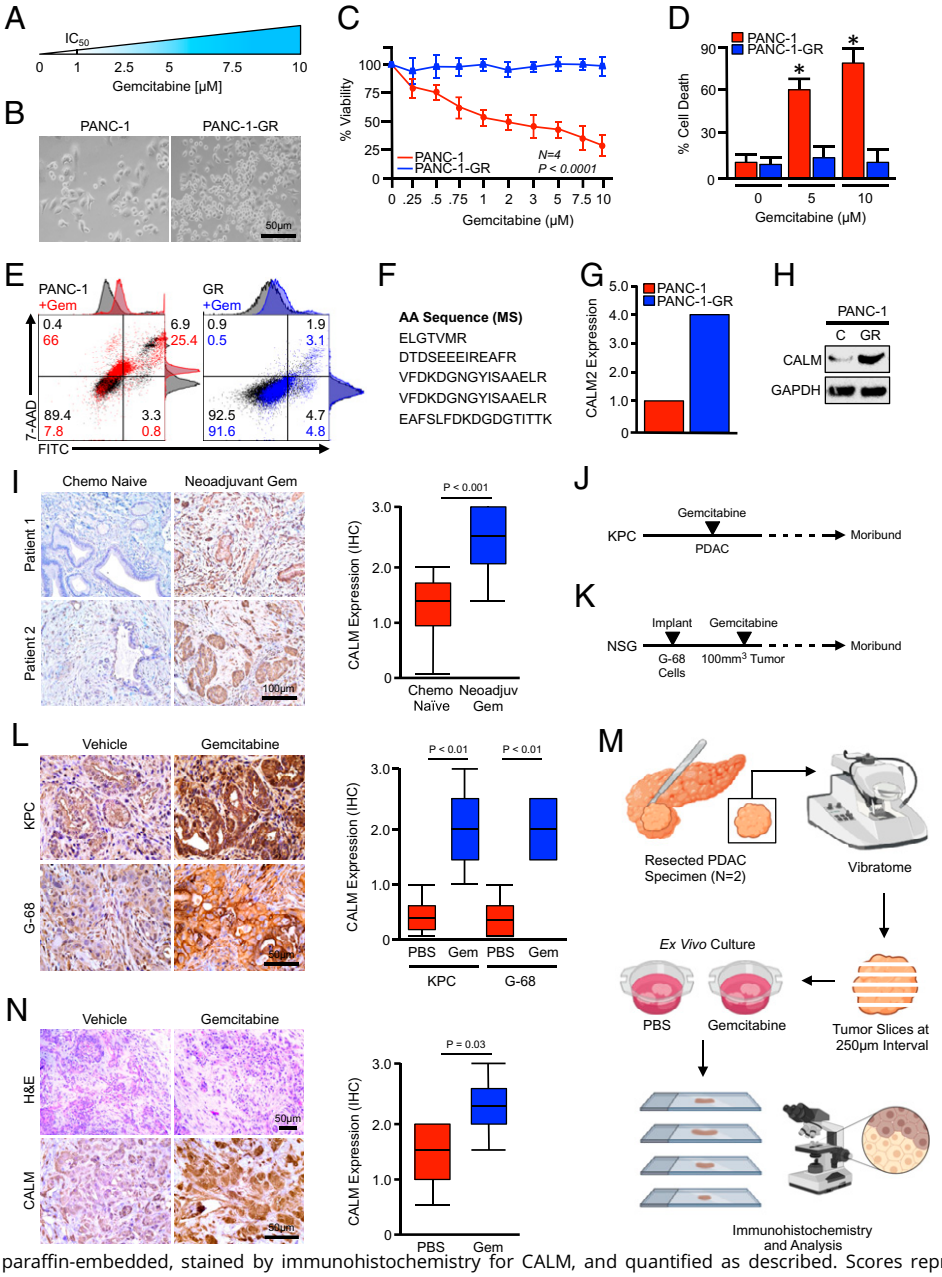

Fig. 2. Calmodulin is frequently overexpressed in GR PDAC. (*A*) PANC-1 tumor cells were incubated with increasing concentrations of gemcitabine until viable in 10 μM. After this point, cells were referred to as PANC-1-GR. (*B*) Low-magnification images of the parental PANC-1 cell line and PANC-1-GR cells. (*C*) PANC-1 and PANC-1-GR cells were incubated with increasing concentrations of gemcitabine and cell viability was evaluated after 48 h by MTT assay. (*D* and *E*) PANC-1 and PANC-1-GR cells were incubated with a saline vehicle, 5 μM gemcitabine, or 10 μM gemcitabine and cell death was evaluated by Annexin-FITC assay. Error bars represent mean ± SEM (*$P < 0.05$). (*F* and *G*) PANC-1 and PANC-1-GR cells were subjected to whole-proteome analysis by 2D gel electrophoresis and mass spectrometry (MS) (see also *SI Appendix*, Fig. S2). This approach revealed the up-regulation of several peptides belonging to the CALM2 protein in PANC-1-GR cells, which were overrepresented nearly fourfold compared with PANC-1 cells. (*H*) Calmodulin expression in PANC-1 and PANC-1-GR cells was evaluated by Western blot. (*I*) Excisional biopsies from 36 PDAC patients were sectioned and stained via immunohistochemistry (IHC) for CALM and representative images are shown for each from either chemotherapy-naïve patients (n = 18) or patients who had received neoadjuvant gemcitabine-based chemotherapy (n = 18). CALM expression was quantified as described, related to chemotherapy status, and displayed as a boxplot. (*J*) Pdx1-Cre × LSL-*Kras*^{G12D} × LSL-*TP53*^{R172H} (KPC) mice were generated as a model of advanced PDAC. Starting at 90 d (~13 wk) of age, mice were administered twice-weekly IP injections of either PBS vehicle or 100 mg/kg gemcitabine. Pancreas tissues were collected when the animals were moribund. (*K*) G-68 human cells were injected subcutaneously into NSG mice and, once tumors reached 100 to 200 mm^3, animals were treated with either a saline vehicle or 40 mg/kg gemcitabine. Animals were killed when moribund or when tumors ulcerated. (*L*) Tissues from vehicle- and gemcitabine-treated mice were stained via immunohistochemistry for CALM and quantified as described. (*M* and *N*) Excisional biopsies from two PDAC patients undergoing survival resection were cored, sectioned at 250-μm intervals, and cultured ex vivo either in a vehicle control or 5 μM gemcitabine. After 72 h, slice cultures were formalin-fixed, paraffin-embedded, stained by immunohistochemistry for CALM, and quantified as described. Scores represent three geographically distinct tumor nests from each patient.

now incorporating pharmacologic inhibitors of MEK-dependent ERK activation in the form of U0126 or PD-98059. In both cases, PANC-1-GR cells became highly gemcitabine-sensitive (Fig. 3*J*). Incubation with W-7 reduced ERK activation in PANC-1-GR cells by immunocytochemistry and in both the calmodulin-low PANC-1 and calmodulin-high PANC-1-GR cells by Western blot (Fig. 3 *K* and *L*). Despite the inhibition of ERK signals in gemcitabine-sensitive cells, W-7 only modestly enhanced the cleavage of caspase 3 (Fig. 3*L*). However, in PANC-1-GR cells, W-7 markedly enhanced the cleavage of caspase 3, consistent with the observed increase in cell death (Fig. 3*L*).

Given these alterations in MAPK signaling, we next explored the relationship between calmodulin and KRAS in this context. As active KRAS signaling occurs at the cell membrane (23), we first restained human tumor tissue for calmodulin and evaluated its localization under high magnification. In most patients, calmodulin was expressed at the cell membrane, with similar results observed in PANC-1-GR cells in vitro (Fig. 3*M*). However, when PANC-1-GR cells were treated with W-7, calmodulin was delocalized from the cell membrane and was more abundant in the cytoplasm (Fig. 3*M*). We next assessed the direct association between calmodulin and KRAS via immunoprecipitation, which affirmed that KRAS coprecipitated calmodulin, though this was strongly inhibited by W-7 (Fig. 3 *N* and *O*). We next evaluated whether this affected RAS activation by incubating samples with a glutathione S-transferase (GST)–tagged RAF1 RAS-binding domain (RBD). RBD–KRAS complexes were immunoprecipitated, resolved, and visualized by Western blot showing a substantial reduction in KRAS activity in W-7–treated cells (Fig. 3*P*).

Finally, to determine if calmodulin is required for ERK activation in human tumor tissue, we again generated slice cultures from two PDAC patients undergoing surgical resection and incubated specimens either with a DMSO vehicle or with W-7.

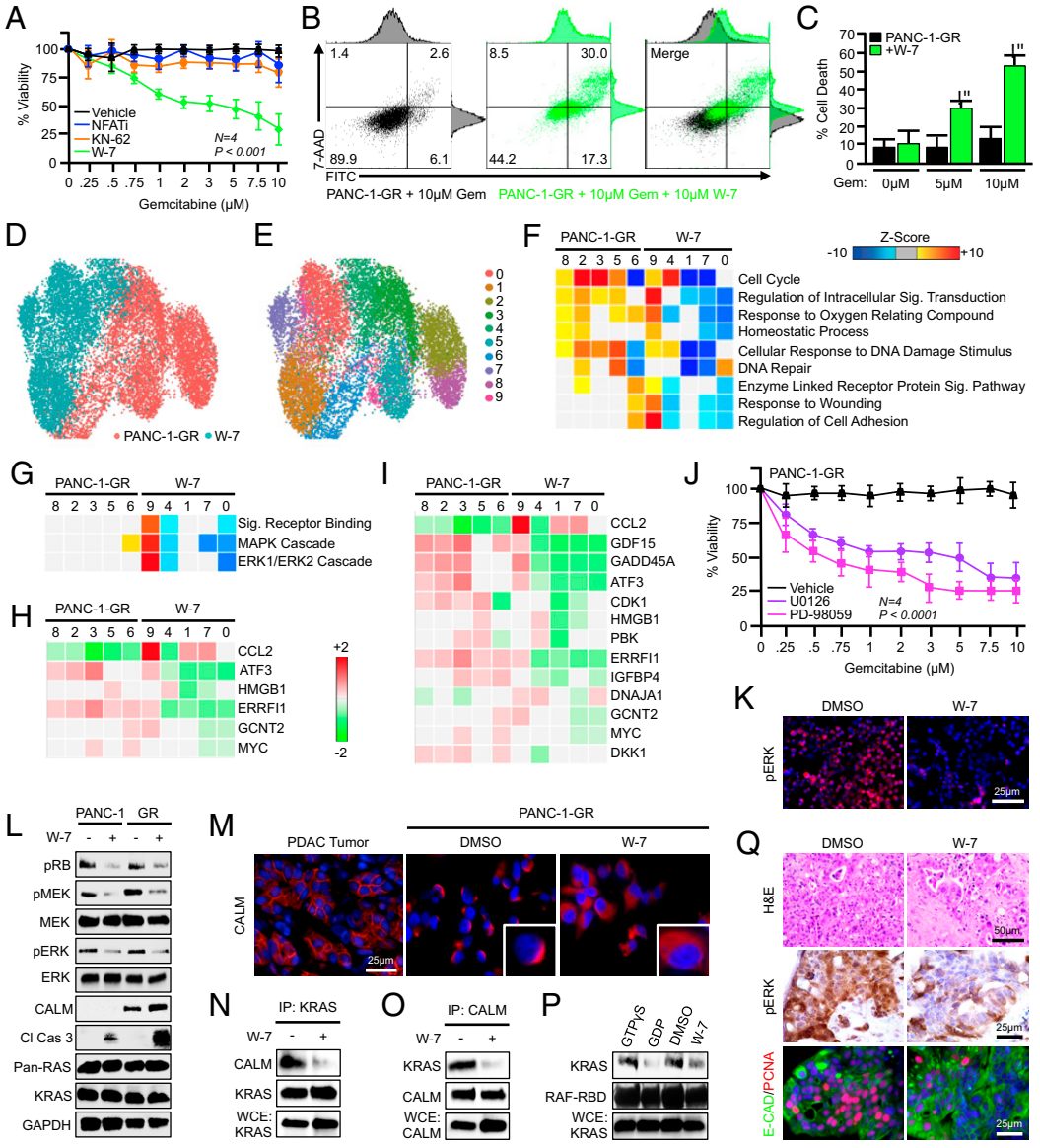

Fig. 3. Calmodulin-dependent ERK activation is required for gemcitabine resistance in vitro. (*A*) PANC-1-GR cells were incubated with a fixed concentration of either a DMSO control (1:1,000), an NFAT-inhibiting peptide (25 μM), the CAMK inhibitor KN-62 (10 μM), or the calmodulin inhibitor W-7 (10 μM). After 2 h, cells were challenged with increasing concentrations of gemcitabine, and cell viability was evaluated after 48 h by MTT assay. Error bars represent mean ± SEM. (*B* and *C*) PANC-1-GR cells were incubated with a DMSO vehicle or 10 μM W-7 followed by 0, 5, or 10 μM gemcitabine, and cell death was evaluated after 48 h by Annexin-FITC assay. Error bars represent mean ± SEM. (*D–F*) PANC-1-GR cells were incubated with a DMSO vehicle or 10 μM W-7 for 24 h, at which time cells were collected and evaluated by single-cell RNA sequencing. Populations were visualized via UMAP scatterplot, transcriptionally distinct clusters were identified, and each was subjected to enrichment analysis for cell processes identified in Fig. 1. (*G*) Cell clusters were interrogated by GiTools for alterations to cell signaling pathways, showing significant down-regulation of MAPK and ERK signaling in W-7–treated clusters. (*H* and *I*) Individual genes in the ERK and MAPK gene sets, respectively. (*J*) PANC-1-GR cells were incubated with a fixed concentration of either a DMSO vehicle (1:1,000) or MEK/ERK inhibitors U0126 (5 μM) or PD-98059 (5 μM). After 2 h, cells were challenged with increasing concentrations of gemcitabine, and cell viability was evaluated after 48 h by MTT assay. Error bars represent mean ± SEM (*$P < 0.05$). (*K*) PANC-1-GR cells were incubated with a fixed concentration of either a DMSO vehicle or W-7 (10 μM), and ERK activation was evaluated by immunochemistry after 24 h. (*L*) PANC-1 and PANC-1-GR cells were treated as described and ERK pathway activation was evaluated by Western blot. (*M*) Human PDAC tumor tissue or PANC-1-GR cells incubated with a DMSO vehicle or W-7 (10 μM) were stained via immunofluorescence for calmodulin. (*N* and *O*) PANC-1-GR cells were again treated with either a DMSO vehicle or W-7, and the interaction between KRAS and CALM was evaluated by immunoprecipitation. WCE, whole-cell extract. (*P*) Following treatment, PANC-1-GR cells were subjected to a KRAS activity assay using an IP with a GST-tagged RBD of the RAF protein. Following IP, complexes were resolved and visualized by Western blot for KRAS. Control and W-7–treated samples were compared with a positive control (GTPγS) and negative control (GDP). (*Q*) Excisional biopsies from two PDAC patients undergoing survival resection were cored, sectioned at 250-μm intervals, and cultured ex vivo either in a control DMSO vehicle or 10 μM W-7. After 72 h, slice cultures were formalin-fixed, paraffin-embedded, and stained either with H&E, via immunohistochemistry for CALM, or dual-stained for CK19 and PCNA.

After 48 h, tissues were stained with hematoxylin and eosin (H&E), via immunohistochemistry for pERK, or dual-stained for the duct marker CK19 and the proliferation surrogate PCNA. Consistent with cell-culture data, W-7–treated tumor slices displayed a substantial reduction in ERK activation, as well as diminished proliferation in CK19-positive tumor nests (Fig. 3*Q*).

Calcium Depletion Disrupts ERK Activation and Restores Gemcitabine Sensitivity In Vitro. As calmodulin inhibitors such as W-7 are not clinically useful, we next sought to determine whether manipulating calcium would mimic the effects of W-7 on drug resistance in PANC-1-GR cells. As previously, PANC-1-GR cells were serum-starved overnight either with control Dulbecco's modified Eagle's medium (DMEM) or

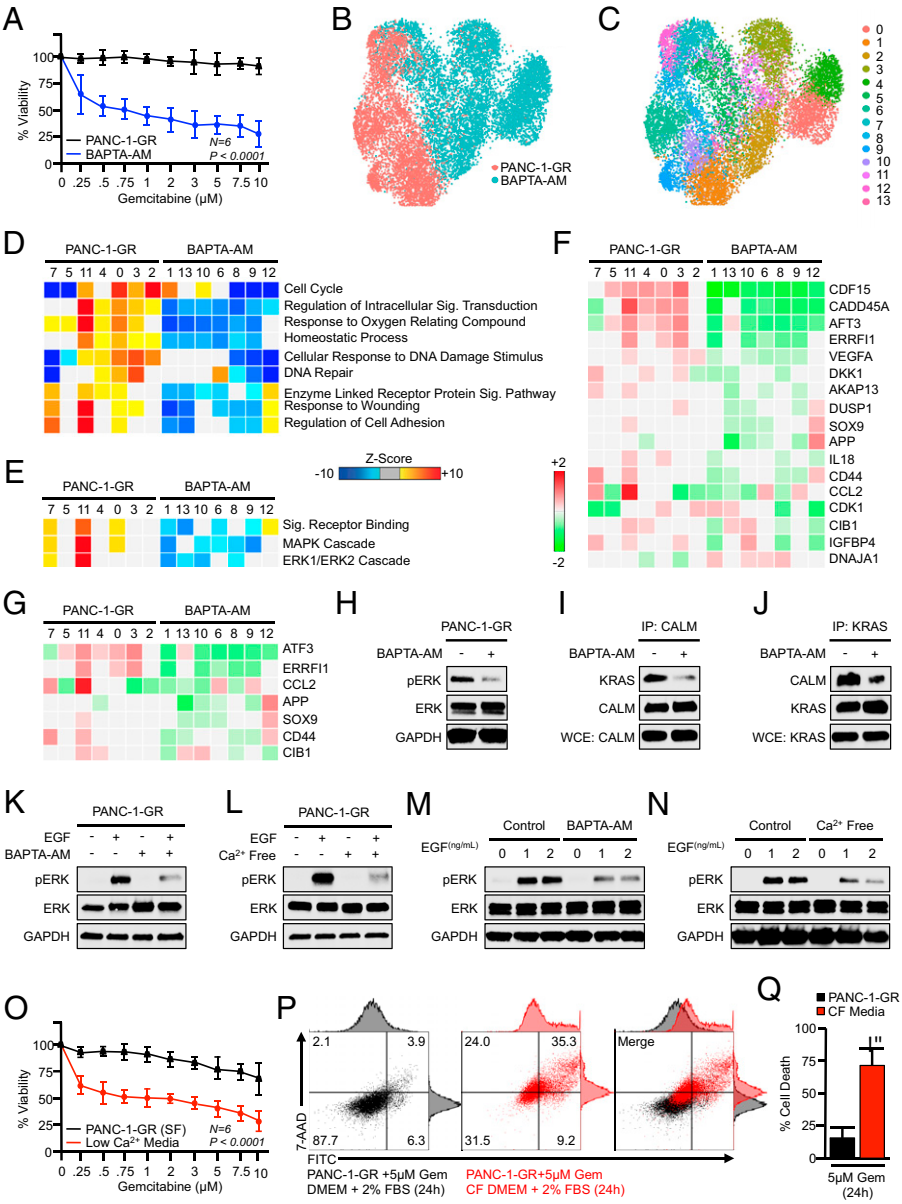

Fig. 4. Calcium depletion disrupts ERK activation and restores gemcitabine sensitivity in vitro. (*A*) PANC-1-GR cells were incubated with a fixed concentration of either a DMSO control (1:1,000) or the calcium chelator BAPTA-AM (10 μM). After 2 h, cells were challenged with increasing concentrations of gemcitabine, and cell viability was evaluated after 48 h by MTT assay. Error bars represent mean ± SEM. (*B–E*) PANC-1-GR cells were treated with either a DMSO vehicle or BAPTA-AM (10 μM) for 24 h. Cells were then collected and evaluated by single-cell RNA sequencing. Cell populations were visualized via UMAP scatterplot, transcriptionally distinct clusters were identified, and each was subjected to enrichment analysis for cell processes and signaling pathways identified previously, with BAPTA-AM–treated clusters showing pronounced down-regulation of MAPK and ERK signaling. (*F* and *G*) Individual genes in the ERK and MAPK gene sets, respectively. (*H*) PANC-1-GR cells were treated with either a DMSO vehicle or BAPTA-AM (10 μM) for 24 h, after which ERK activation was assayed by Western blot. (*I* and *J*) PANC-1-GR cells were treated similarly, and the interaction between KRAS and CALM was evaluated by immunoprecipitation. (*K* and *L*) PANC-1-GR cells were incubated with either a DMSO vehicle or BAPTA-AM in serum-free media for 24 h. Cells were then stimulated with 0.5 ng/mL recombinant EGF, and ERK activation was evaluated by Western blot after 10 min. The experiment was then repeated using cells grown in either control serum-free media or calcium (Ca^{2+})-free, serum-free media. (*M* and *N*) This experiment was repeated using 0, 1, or 2 ng/mL EGF. (*O*) PANC-1-GR cells were cultured overnight in either unmodified serum control, serum-free media, or Ca^{2+}-free, serum-free media. At this time, cells were challenged with increasing concentrations of gemcitabine, and cell viability was evaluated after 24 h by MTT assay. Error bars represent mean ± SEM. (*P* and *Q*) PANC-1-GR cells were grown in either control media supplemented with 2% FBS or Ca^{2+}-free (CF) media with 2% FBS (low-Ca^{2+} media) and cell death was evaluated by Annexin-FITC assay. Error bars represent mean ± SEM (*$P < 0.05$).

DMEM supplemented with the calcium chelator BAPTA-AM (10 μM). Cells were then changed to medium containing 10% fetal bovine serum (FBS) with or without BAPTA-AM, as well as varying doses of gemcitabine. After another 48 h, cell viability was evaluated by MTT assay. Consistent with our observations using W-7, BAPTA-AM led to the loss of gemcitabine resistance, which reduced cell viability in a dose-dependent manner (Fig. 4*A*). We next treated PANC-1-GR cells as previously and, after 24 h, conducted single-cell RNA sequencing. Cells were again displayed via UMAP dimensionality reduction and clustered as earlier described.

Using this approach, untreated PANC-1-GR cells were represented by seven well-defined clusters with seven additional clusters for BAPTA-AM–treated PANC-1-GR cells (Fig. 4 *B* and *C*). We again conducted enrichment analysis for genes in relation to GO biological processes in each cluster, revealing a significant down-regulation in several of the same cell processes affected by W-7, especially those involved in the cell cycle (Fig. 4*D*). When evaluating GO gene sets associated with cell signaling, we again observed a significant down-regulation in the GO signal receptor binding pathway gene set, as well as most genes in the GO MAPK and ERK1/2 cascade gene sets (Fig. 4 *E–G*). The BAPTA-AM–mediated inhibition of ERK activation was next confirmed by Western blot (Fig. 4*H*) and, like W-7, BAPTA-AM–mediated calcium chelation disrupted the formation of calmodulin/KRAS formation as determined by immunoprecipitation experiments (Fig. 4 *I* and *J*).

To further evaluate whether calcium is necessary for ERK activation, we next conducted a series of experiments in serum-free media, utilizing recombinant EGF as a positive stimulus for ERK activation. We first serum-starved PANC-1-GR cells overnight with either control DMEM or DMEM plus BAPTA-AM and stimulated cells with 0.5 ng/mL recombinant EGF. After 10 min, ERK activation was evaluated by Western blot. Low-dose EGF strongly enhanced ERK phosphorylation in control serum-free media, though this was not observed in BAPTA-AM–containing media (Fig. 4*K*). We repeated these experiments using DMEM lacking calcium and observed similar results with poor ERK activation under calcium-free conditions (Fig. 4*L*). These experiments were repeated using higher doses of EGF (1 to 2 ng/mL). Under these conditions, EGF noticeably induced ERK phosphorylation in BAPTA-AM–supplemented or calcium-free media, though this

activation was weaker than in control media (Fig. 4 *M* and *N*). Given the effect of calcium-free media on ERK activation, we next repeated cell-viability assays as described, now using either control serum-free media supplemented with 2% FBS or calcium-free media supplemented similarly (low-calcium media). Similar to results using BAPTA-AM, cells grown in low-calcium media were poorly drug-resistant with reduced viability across all doses of gemcitabine after 24 h (Fig. 4*O*), and displayed increased apoptosis when administered a 5 μM dose (Fig. 4 *P* and *Q*).

Calcium Channel Blockers Impair Prosurvival ERK Signaling and Improve Gemcitabine Sensitivity In Vitro. Based on retrospective observations that PDAC patients receiving CCBs display improved therapeutic responses to gemcitabine-based chemotherapy (17), we hypothesized that CCBs might provide a clinically useful means to deplete intracellular calcium, thereby interrupting calmodulin-induced ERK activation and improving therapeutic responses. We therefore stained the 36 excisional biopsies from PDAC patients for LTCCs, the primary target of CCBs (24) (Fig. 5*A*). LTCCs were ubiquitous to both chemotherapy-naïve and chemotherapy-treated patients (Fig. 5*B*), and were expressed in several PDAC cell lines, including PANC-1-GR, which localized exclusively to the cell membrane (Fig. 5 *C* and *D*).

We next serum-starved PANC-1-GR cells overnight and pretreated with either a DMSO control or the CCBs nifedipine or amlodipine (5 μM). After 2 h, cells were changed to full-serum media containing the same treatments and increasing concentrations of gemcitabine. After another 48 h, cell viability was evaluated by MTT assay. In PANC-1-GR cells treated with either nifedipine or amlodipine, gemcitabine reduced cell viability in a dose-dependent manner (Fig. 5*E*), and sensitized cells to gemcitabine-induced apoptosis when subjected to Annexin-FITC (fluorescein isothiocyanate) assay (Fig. 5*F*). Similar results were observed using gemcitabine-naïve PANC-1, MiaPaCa-2, and ASPC-1 cells (*SI Appendix*, Fig. S3).

To identify the underlying mechanism, PANC-1-GR cells were again treated with amlodipine and compared with untreated controls after 24 h by single-cell RNA sequencing. Cells were again displayed via UMAP dimensionality reduction and clustered as described (Fig. 5*G*). These amlodipine-treated PANC-1-GR cells demonstrated high transcriptional similarity to W-7– and BAPTA-AM–treated cells, all of which were significantly different from the controls, particularly for genes related to the cell cycle (*SI Appendix*, Figs. S4 and S5). When this comparison was restricted to control and amlodipine-treated cells, untreated PANC-1-GR cells were represented by five clusters, and amlodipine-treated cells by an additional five clusters (Fig. 5*H*).

We again conducted enrichment analysis in these clusters for genes in relation to GO biological processes in each cluster, revealing a significant down-regulation in several of the same cell processes affected by W-7 and BAPTA-AM in the amlodipine groups, including genes involved in cell-cycle progression (Fig. 5*I*). We found that most amlodipine-treated cells showed inhibition of several pathways involved in calcium ion transport, closely mimicking results using BAPTA-AM (*SI Appendix*, Fig. S6). Also, as previously, amlodipine-treated cells displayed profound suppression of MAPK and ERK1/ERK2 cascades (Fig. 5*J*), with nearly all drug-associated clusters showing a pronounced down-regulation of previously identified genes in the MAPK and ERK pathways (Fig. 5 *K* and *L*). At the protein level, amlodipine treatment inhibited the direct association between calmodulin and KRAS as determined by immunoprecipitation (Fig. 5*M*), and treatment with either nifedipine or amlodipine impaired ERK pathway activation by Western blot (Fig. 5*N*), with similar results observed in chemotherapy-naïve MiaPaCa-2 and ASPC-1 cell lines (Fig. 5 *O* and *P*). As ERK is central to cell survival, we also examined the effects of nifedipine and amlodipine on responses to several other chemotherapy medications used in PDAC and found that the CCBs ubiquitously enhanced chemotherapy sensitivity in PANC-1, MiaPaCa-2, and ASPC-1 cells (*SI Appendix*, Fig. S7).

To translate these findings to tumor tissues, we again generated slice cultures from two PDAC patients undergoing surgical resection and incubated specimens either with a DMSO vehicle, nifedipine, or amlodipine. After 48 h, tissues were stained with H&E, via immunohistochemistry for pERK, or dual-stained for the duct marker CK19 and the proliferation surrogate PCNA. As previously, tumor slices treated with either nifedipine or amlodipine displayed a substantial reduction in ERK activation, as well as diminished proliferation in CK19-positive tumor nests (Fig. 5*Q*).

Amlodipine Extends Survival in Orthotopic Xenografts of GR PDAC Cells. To determine the in vivo efficacy of amlodipine as an adjunct therapy in GR PDAC, we transfused PANC-1-GR cells with luciferase (PANC-1-GR^{Luc}) and implanted 0.8×10^6 cells into the pancreas of NSG mice (Fig. 6*A*). Disease progression was monitored by In Vivo Imaging System (IVIS), and once animals developed 100-mm^3 tumors, they were enrolled into one of four treatment groups. Mice were given IP injections of a PBS vehicle ($n = 5$), 100 mg/kg gemcitabine twice per week ($n = 7$), 2.5 mg/kg amlodipine daily ($n = 5$), or twice weekly gemcitabine with daily injections of amlodipine ($n = 9$). Mice were killed when showing clear signs of health decline, such as weight loss or lethargy, at which time tissues were collected and subjected to histopathology (Fig. 6*B*). Consistent with the GR phenotype, mice treated with gemcitabine had no statistically significant survival advantage compared with vehicle-treated controls. Additionally, amlodipine monotherapy also failed to alter disease outcomes. However, mice treated with both gemcitabine and amlodipine had significantly enhanced survival, with 5/10 mice reaching the study end point of 100-d postenrollment (Fig. 6*C*).

On dissection, 5/5 control mice had extensive nodular masses throughout a firm, enlarged pancreas, as did 6/6 gemcitabine-treated mice and 5/5 amlodipine-treated mice. Additionally, 4/5 control mice developed extensive hepatic and splenic metastases, as did 6/7 gemcitabine-treated mice and 5/5 amlodipine-treated mice (Fig. 6*D* and *SI Appendix*, Fig. S8). However, only 3/9 mice treated with gemcitabine and amlodipine had large, frank tumors throughout the pancreas, and only 1/9 developed liver metastases (Fig. 6 *D*–*F*). Consistent with our in vitro data, pancreatic tumors treated with the combination of gemcitabine and amlodipine had little ERK activation compared with all other groups, paralleled by a substantial reduction in proliferation (Fig. 6 *G* and *H*).

Amlodipine Potentiates Gemcitabine Chemotherapy in KPC Mice. While amlodipine has clear efficacy as a gemcitabine adjunct in xenografted tumor cells, these experiments are limited, as these tumors do not resemble clinically relevant human PDAC histotypes. Further, these xenografted tumors lack the dense, fibroinflammatory reaction that is a hallmark of PDAC and rely on immunocompromised mice. We therefore used the well-accepted Pdx1-Cre × LSL-*KRAS*^{G12D} × LSL-*TP53*^{R172H} (KPC) mouse model of autochthonous PDAC. As described in the original reference, KPC animals develop pancreatic

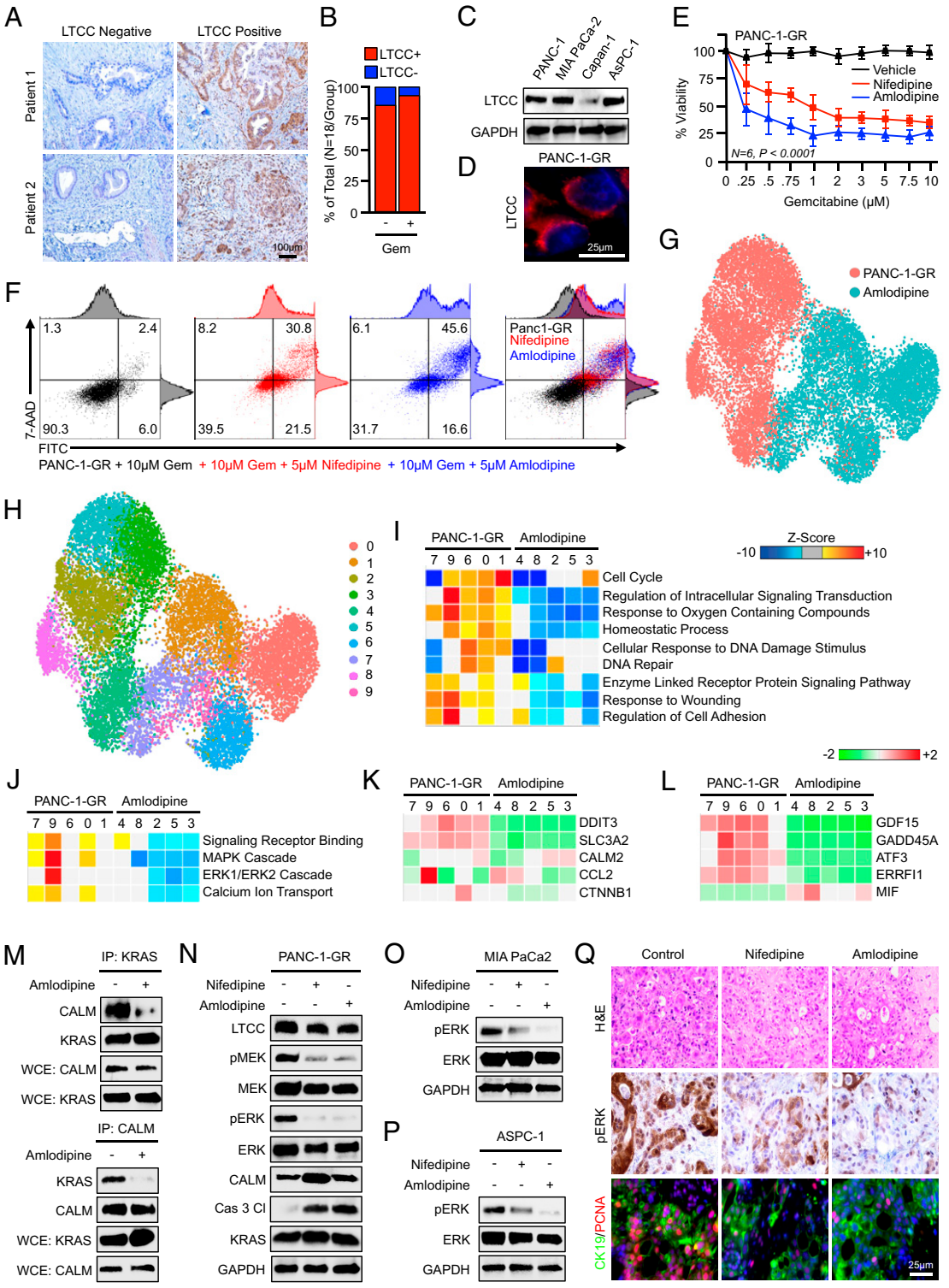

Fig. 5. Calcium channel blockers impair prosurvival ERK signaling and improve gemcitabine sensitivity in vitro. (*A*) Excisional biopsies from 36 PDAC patients were sectioned and stained via immunohistochemistry for LTCCs and representative images are shown for each from either chemotherapy-naïve patients (n = 18) or patients who had received neoadjuvant gemcitabine-based chemotherapy (n = 18). (*B*) The percentage of patients in each group with LTCC-expressing and non–LTCC-expressing tumors. (*C*) PANC-1, MiaPaCa-2, Capan-1, and ASPC-1 cells were evaluated for LTCC expression by Western blot. (*D*) PANC-1-GR cells were stained for LTCCs by immunofluorescence, showing strong membrane localization. (*E*) PANC-1-GR cells were incubated with a fixed concentration of either a DMSO vehicle (1:1,000) or the CCBs nifedipine (5 μM) or amlodipine (5 μM). After 2 h, cells were challenged with increasing concentrations of gemcitabine, and cell viability was evaluated after 48 h by MTT assay. Error bars represent mean ± SEM. (*F*) PANC-1-GR cells were treated similarly and cell death was evaluated by Annexin-FITC assay. (*G–J*) PANC-1-GR cells incubated with either a DMSO control vehicle or amlodipine (5 μM) for 24 h. Cells were then collected and evaluated by single-cell RNA sequencing. Cell populations were visualized via UMAP scatterplot, transcriptionally distinct clusters were identified, and each was subjected to enrichment analysis for cell processes identified in Fig. 1, with amlodipine-treated clusters showing significant down-regulation of MAPK and ERK signaling. (*K* and *L*) Individual genes in the ERK and MAPK gene sets, respectively. (*M* and *N*) PANC-1-GR cells were treated similarly, and the interaction between KRAS and calmodulin was evaluated by immunoprecipitation. Cell lysate was also evaluated by Western blot for ERK pathway activation. (*O* and *P*) MiaPaCa-2 and ASPC-1 cells were treated with nifedipine (5 μM) or amlodipine (5 μM), and ERK activation was evaluated by Western blot. (*Q*) Excisional biopsies from two PDAC patients undergoing survival resection were cored, sectioned at 250-μm intervals, and cultured ex vivo either in a control DMSO vehicle, nifedipine (5 μM), or amlodipine (5 μM). After 72 h, slice cultures were formalin-fixed, paraffin-embedded, and stained either with H&E, via immunohistochemistry for CALM, or dual-stained for CK19 and PCNA.

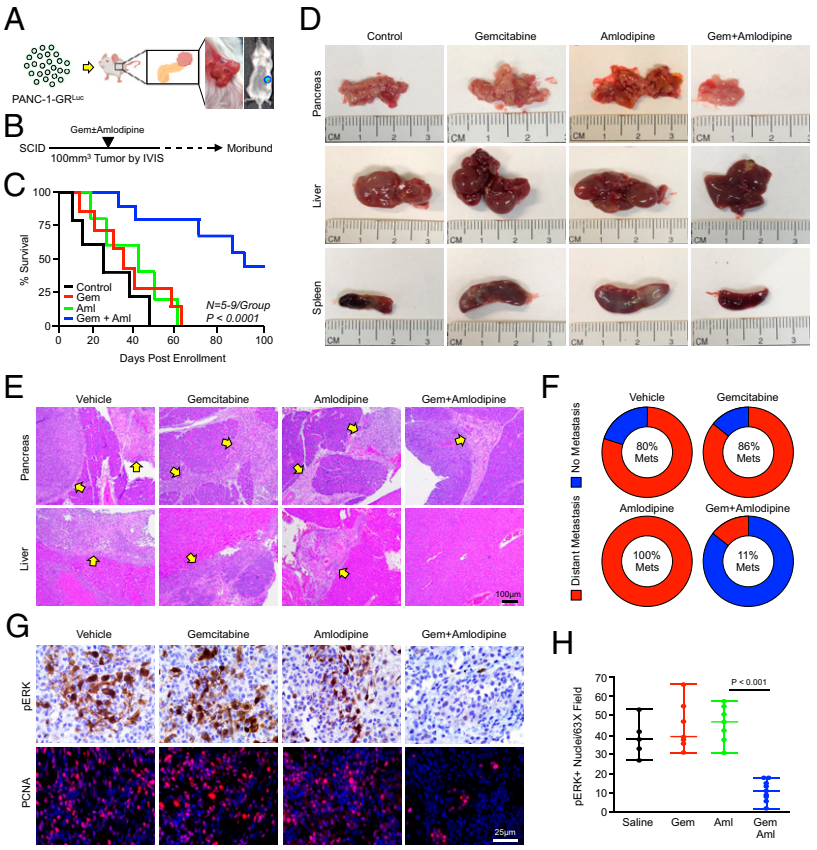

Fig. 6. Amlodipine extends survival in orthotopic xenografts of GR tumor cells. (*A–C*) PANC-1-GR cells were transduced with stable expression of firefly luciferase (PANC-1-GR^{Luc}), and 0.8 × 10^6 cells were implanted into the pancreas of NSG mice. Disease progression was monitored by IVIS, and once animals developed 100-mm^3 tumors, they were enrolled into one of four treatment groups. Mice were given IP injections of a PBS vehicle (n = 5), 100 mg/kg gemcitabine twice per week (n = 7), 2 mg/kg amlodipine daily (n = 5), or twice weekly gemcitabine with daily injections of amlodipine (n = 9). Mice were killed when showing clear signs of health decline such as weight loss or lethargy, and survival is shown via the Kaplan–Meier method. (*D*) At the study end point, gross changes in the pancreas, liver, and spleen were evaluated and representative images are shown for each group. (*E*) Tissues also were stained with H&E, and representative images are shown for tumors in the pancreas and liver. Arrows point to areas of tumor tissues. (*F*) The percentage of mice in each group showing metastatic lesions to the liver, spleen, and/or body wall. (*G* and *H*) Tissues were stained with H&E or via immunohistochemistry for pERK or PCNA and quantified as described, and results are displayed as individual value plots.

intraepithelial neoplasms at 6 wk, focal PDAC at 15 wk, and advanced PDAC at 18 wk (25). Thus, in this study, animals were allowed to develop overt disease for a minimum of 3.5 mo, at which point 100% of mice in our colony have developed locally invasive PDAC (20). After verifying the expression of LTCCs in murine PDAC by immunohistochemistry (Fig. 7*A*), we randomized mice at a 50:50 male-to-female ratio into one of four treatment groups. Mice were either treated with IP injections of a saline vehicle, 100 mg/kg gemcitabine twice per week, daily injections of 2 mg/kg amlodipine, or twice weekly gemcitabine with daily IP injections of 2 mg/kg amlodipine. As previously, mice were killed when showing clear signs of health decline such as weight loss or lethargy, at which time tissues were collected and subjected to histopathology (Fig. 7*B*).

Consistent with our previous observations (20), KPC mice treated with gemcitabine monotherapy had a very modest survival advantage. Similar to results using orthotopic xenografts, amlodipine failed to extend survival beyond that of saline-treated mice, though the combination of gemcitabine and amlodipine had a significant survival advantage compared with all other groups (Fig. 7*C* and *SI Appendix*, Fig. S9*A*). On necropsy, the pancreas from mice in the combination arm was generally smaller, softer, and displayed a reduced incidence of nodular tumors throughout. This corresponded to a significant reduction in the weight of the pancreas, particularly when normalized to body weight (Fig. 7*D* and *SI Appendix*, Fig. S9*B*).

On histologic evaluation, single-agent gemcitabine or amlodipine failed to significantly alter the gland architecture when compared with saline-treated controls (Fig. 7 *E–G* and *SI Appendix*, Fig. S9 *C–E*). However, consistent with the reduction in gland weight, the majority of mice treated with both gemcitabine and amlodipine had at least some preservation of normal gland architecture, as well as a reduction in the number of lesions per high-power field and tumor-associated fibrosis (Fig. 7 *E–H*). While single-agent amlodipine failed to significantly reduce ERK activation at the study end point, mice in the combination arm displayed reduced ERK activation with parallel reductions in proliferation and enhanced apoptosis (Fig. 7 *I–K* and *SI Appendix*, Fig. S9 *F–H*).

Discussion

For decades, gemcitabine has remained one of the most important and widely used medications in the treatment of PDAC. Though gemcitabine-based chemotherapy provides a modest survival in both the first- and second-line setting, nearly all tumors will eventually experience disease progression and long-term survivability remains poor. Though gemcitabine resistance is well-documented in the clinic, the cellular and molecular mechanisms that underlie GR phenotypes remain unclear. Though several possible mechanisms have been suggested, none has successfully translated to a clinically useful combination

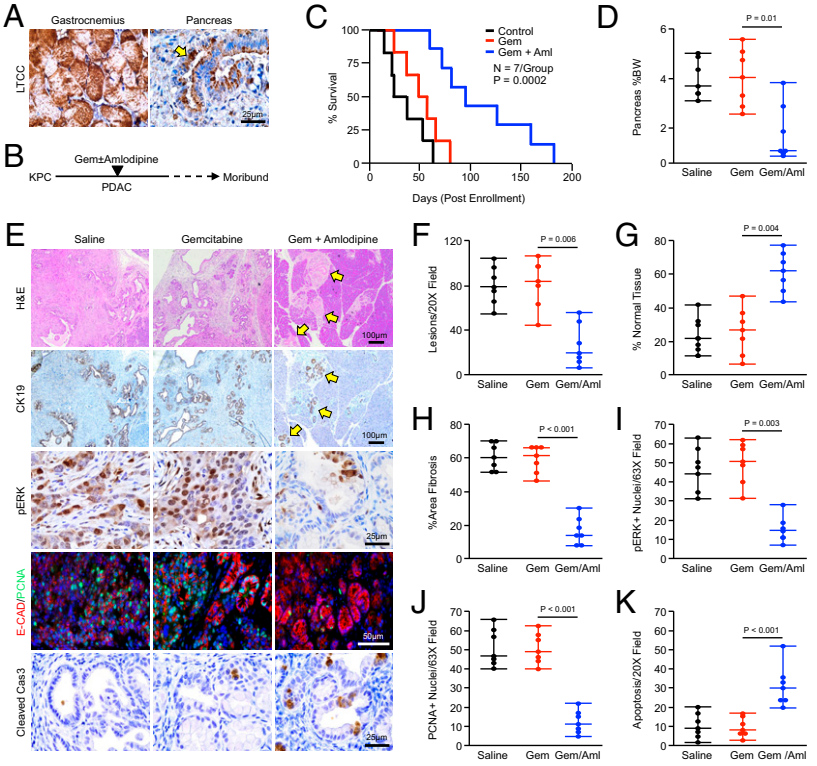

Fig. 7. Amlodipine potentiates gemcitabine chemotherapy in KPC mice. (*A*) Pdx1-Cre × LSL-*Kras*^{G12D} × LSL-*TP53*^{R172H}(KPC) mice were generated as a model of advanced PDAC. Pancreas tissues were collected from tumor-bearing mice, sectioned, and stained via immunohistochemistry for LTCCs, with muscle tissue from the gastrocnemius used as a positive control. The arrows indicate LTCC-expressing neoplastic tissues. (*B* and *C*) Starting at 15 wk of age, KPC mice were enrolled into one of four treatment groups. Mice were either treated with IP injections of a saline vehicle, 100 mg/kg gemcitabine twice per week, daily injections of 2 mg/kg amlodipine, or gemcitabine and amlodipine. Mice were killed when showing clear signs of health decline such as weight loss or lethargy, and survival is shown via the Kaplan–Meier method. For the amlodipine monotherapy group, see *SI Appendix*, Fig. S9*A*. (*D*) At the study end point, the pancreas gland was weighed and normalized to each animal's body weight (BW), and results are displayed as individual value plots. For the amlodipine monotherapy group, see *SI Appendix*, Fig. S9*B*. (*E–K*) Pancreas tissues were stained with H&E or via immunohistochemistry for CK19, pERK, E-cadherin and PCNA, or cleaved caspase 3. Tissues were quantified as described and results are displayed as individual value plots. For the amlodipine monotherapy group, see *SI Appendix*, Fig. S9 *C–H*.

strategy to reverse gemcitabine resistance or prolong its therapeutic efficacy.

As mentioned, PDAC tumors frequently overexpress EGFR, which has been linked to gemcitabine resistance through the transactivation of antiapoptotic PI3K/AKT signaling (4). Despite the promise of this approach in preclinical studies, the addition of the EGFR inhibitor erlotinib to gemcitabine monotherapy extended median overall survival by less than 2 wk in a phase III trial (5). Given the lack of a more effective treatment option, erlotinib was approved for this indication by the FDA. In the years since, several other targeted therapies have been combined with gemcitabine in clinical trials, in most instances with strong scientific rationale. However, progress has been difficult and, at this time, no additional treatment strategy has earned FDA approval.

Notable examples include the EGFR inhibitor cetuximab, which failed to significantly improve survival when combined with gemcitabine-based chemotherapy (26). Similarly, though the addition of VEGF signaling inhibitors bevacizumab and axitinib showed early promise in combination with gemcitabine-based chemotherapy in phase II trials, neither combination showed a meaningful clinical benefit in phase III testing (7, 8). In addition to VEGF, Hedgehog/Smoothened signaling has been directly implicated in gemcitabine resistance in PDAC via the downstream activation of GLI-SOX2 signaling (27). However, the Smoothened inhibitor vismodegib also failed to improve outcomes when added to gemcitabine in a clinical trial (6).

In this study, we explored potential means of escape from gemcitabine-induced apoptosis via a combination of single-cell RNA sequencing and high-throughput proteomic analysis. These data appeared to implicate aberrations in calcium-dependent calmodulin signaling in gemcitabine resistance. Specifically, cell lines, animal models, and human PDAC tissues showed an increase in the expression of CALM2 following long-term treatment with gemcitabine, often accumulating at the cell membrane. Pharmacologic ablation of calcium-dependent calmodulin activation was sufficient to reverse gemcitabine resistance in vitro, which subsequent analyses determined was through the inhibition of prosurvival ERK and MAPK signaling. This is consistent with previous observations demonstrating that ERK signaling is central to gemcitabine resistance in PDAC (13, 14, 28). However, the relationship between calmodulin and ERK activation is poorly understood and appears to be highly context-dependent.

In KRAS-driven cancers such as PDAC, calmodulin has contradictory roles in directing the activation of the MEK/ERK and PI3K/AKT pathways (29). For example, consistent with our observations, the KRAS4b isoform has been shown to interact with calmodulin in a prenylation-dependent and nucleotide-independent manner (30), though this association does appear to require calcium (31, 32). While this interaction has been known for years, its biological consequences are controversial, involving additional signaling effectors that operate in a highly context-specific manner. For example, phosphorylated calmodulin can

potentiate KRAS-induced activation of PI3K/AKT signaling, tightening the binding between KRAS4b and PI3Kα (33). This appears to also involve association with the IQ domain GTPase-activating scaffolding protein 1 (IQGAP1), which associates with calcium-bound calmodulin and contributes to KRAS-dependent activation of PI3K at the cell membrane (34, 35). Further complicating these events, conformational ensembles of KRAS4B–calmodulin complexes are diverse, often involving additional posttranslational modifications such as farnesylation and methylation (36).

Though there is a growing body of evidence suggesting that calmodulin can potentiate KRAS-induced activation of PI3K/AKT signaling in epithelial cells (37), data regarding calmodulin and ERK are less clear. In fibroblasts, calmodulin can directly bind to KRAS to inhibit downstream activation of RAF/MEK/ERK (38) and inhibit KRAS phosphorylation at the hypervariability region (39). This has been suggested to inhibit the sustained high activation of ERK following stimulation by growth factors, preserving the proliferative effect of the KRAS/ERK pathway (40). While similar results have been observed in other model systems, several other studies support a role for calmodulin in enhancing KRAS-induced ERK activation. In pheochromocytoma cells, pharmacologic inhibition of calmodulin via W-13 or calmidazolium prevented the activation of both ERK and p38 MAPK (41).

Many studies have focused on the role of calmodulin-dependent kinases in facilitating ERK activation (42, 43); others suggest a more direct role for calmodulin in RAS activation. For example, the EGF-responsive MAPK scaffold protein kinase suppressor of Ras1 (KSR1) has been shown to rewire calmodulin signaling in hepatocytes, coupling calcium-dependent calmodulin activation to ERK activation (44). In this study, calcium was required for the association between calmodulin and KSR1, and calcium chelation substantially reduced EGF-induced ERK activation in KSR1-expressing cells (44). This is consistent with prior observations that pretreating hepatocytes with calcium chelators or calmodulin inhibitors, including W-7, markedly reduces ERK activation (45). In PDAC cells, little is known regarding the role of calmodulin and ERK activation, though early evidence supports a role for calmodulin in enhancing ERK activation in PANC-1 cells, in part via cross-talk with SRC kinase (46). Hence, though there is consensus that many adenocarcinomas are dependent on calcium/calmodulin signaling (29, 47–50), our study raises important questions regarding the intersection between calmodulin and the KRAS/ERK pathway in PDAC, which warrants continued exploration.

Nevertheless, though the exact means through which calmodulin contributes to KRAS/ERK activation in PDAC cells remain unclear, our data suggest that calcium-dependent calmodulin signaling protects tumor cells from gemcitabine-induced apoptosis. Accordingly, GR PDAC cells appear highly sensitive to adjuvant therapies targeting calcium. As mentioned, this is consistent with retrospective clinical data demonstrating that PDAC patients receiving amlodipine had improved survival when receiving gemcitabine-based chemotherapy (17). This is supported by a more recent retrospective study, which determined that PDAC patients receiving a CCB had a median overall survival of 15.3 mo compared with 10.1 mo for patients without a CCB. Though encouraging, this study did not restrict treatment to gemcitabine-based chemotherapy and is suggestive rather than definitive (51). Hence, no studies to date, either preclinical or clinical, have evaluated the CCBs to gemcitabine-based chemotherapy in a controlled setting.

Several studies have, however, investigated the effects of CCBs on tumor cells, some also related to drug resistance. For example, CCBs have been shown to reverse docetaxel- and vincristine-induced multidrug resistance in non–small-cell lung cancer cells in a transporter-independent manner (52, 53). Recently, the LTCC subunit *CACNG4* has been shown to be up-regulated in aggressive breast cancers, increasing both cell proliferation and migratory capacity (54). In gastric cancer, both amlodipine and verapamil have been shown to restrain tumor growth in vivo, particularly when combined with cisplatin chemotherapy (55). Interestingly, the CCBs amlodipine and lercanidipine impede ERK activation in gastric cancer cells, cooperating with doxorubicin to induce cell death (56). In PDAC, while CCB-induced cell death has been reported (57), relatively little is known regarding LTCC biology. While most PDAC cell lines appear CCB-sensitive with respect to proliferation (58), *KRAS*-mutated cells appear to be particularly sensitive to CCB-induced apoptosis, blocking KRAS membrane localization and activation (59). At present, there has yet to be a randomized clinical trial exploring whether the addition of a CCB can extend survival beyond placebo for patients receiving gemcitabine-based chemotherapy. Therefore, this strategy may warrant more careful clinical investigation, particularly given the favorable toxicity profile, low cost, and ready availability of CCBs such as amlodipine.

Materials and Methods

Transgenic Mice. Pdx1-Cre × LSL-*Kras*^{G12D} × LSL-*TP53*^{R172H} (KPC) mice were generated as described in our previous work (20, 60, 61). At roughly 3.5 mo of age, KPC mice were administered an IP injection of a PBS vehicle, gemcitabine (100 mg/kg), amlodipine (2 mg/kg), or the combination of gemcitabine and amlodipine. KPC mice were killed when moribund or showing clear signs of health decline, such as fur loss, weight loss, or lethargy, or when they reached 8 mo of age in the case of mice with prolonged survival. For euthanasia, animals were anesthetized with isoflurane until unresponsive to toe tap and/or agonal breathing. Thoracotomy served as the primary method of euthanasia and exsanguination the secondary method. For all mouse studies, males and females were randomized at a 50:50 ratio.

Statistical Analysis. Nonsequencing, nonsurvival data were analyzed by two-way ANOVA and fit to a general linear model in Minitab16, the validity of which was tested by adherence to the normality assumption and the fitted plot of the residuals. Results were arranged by the Tukey method, and were considered significant at $P < 0.05$. Results are presented as mean ± SEM unless otherwise noted. Survival data were analyzed by the Kaplan–Meier/log-rank test method as described previously (62).

Study Approval. All experiments involving the use of mice were performed following protocols approved by the Institutional Animal Care and Use Committee at the University of Illinois at Chicago. Patient slides and information were obtained from patients who provided full written informed consent. This was then deidentified by the Northwestern University Pathcore or the University of Florida, both in accordance with local institutional review board approval.

Data Availability. Data have been deposited in Gene Expression Omnibus (GSE186960). All other study data are included in the article and/or *SI Appendix*.

ACKNOWLEDGMENTS. This work was supported by Veterans Affairs Merit Award I01BX004903 and Career Scientist Award IK6BX004855 (to A.R.), and Veterans Affairs Merit Awards BX003296 and BX005791 (to B.R.). It is partially supported by NIH F30CA236031 and the University of Illinois at Chicago Award for Graduate Research (to D.R.P.), NIH R21CA255291 and Veterans Affairs Merit Award I01BX002922 (to H.G.M.), NIH R01CA242003 and the Joseph and Ann Matella Fund for Pancreatic Cancer Research (to J.G.T.), and NIH R01CA211095 (to E.V.B.). We thank Drs. Dinesh Thummuri and Zhou Daohong for providing tissues from the G-68 CDX model. The contents of this article are the responsibility of the authors and do not represent the views of the Department of Veterans Affairs or the US Government.

Author affiliations: [a]Medical Scientist Training Program, University of Illinois College of Medicine, Chicago, IL 60612; [b]Department of Surgery, University of Illinois at Chicago, Chicago, IL 60612; [c]Department of Biochemistry and Molecular Genetics, University of Illinois at Chicago, Chicago, IL 60612; [d]Department of Medicine, Feinberg School of Medicine, Northwestern University, Evanston, IL 60611; [e]Department of Surgery, University of Florida College of Medicine, Gainesville, FL 32611; [f]Division of Surgical Oncology, Department of Surgery, Virginia Commonwealth University, Richmond, VA 23284; and [g]Jesse Brown VA Medical Center, Chicago, IL 60612

1. D. R. Principe *et al.*, The current treatment paradigm for pancreatic ductal adenocarcinoma and barriers to therapeutic efficacy. *Front. Oncol.* **11**, 688377 (2021).
2. D. P. Sohal, P. B. Mangu, D. Laheru, Metastatic pancreatic cancer: American Society of Clinical Oncology clinical practice guideline summary. *J. Oncol. Pract.* **13**, 261–264 (2017).
3. A. Wang-Gillam *et al.*, NAPOLI-1 phase 3 study of liposomal irinotecan in metastatic pancreatic cancer: Final overall survival analysis and characteristics of long-term survivors. *Eur. J. Cancer* **108**, 78–87 (2019).
4. S. S. Ng, M. S. Tsao, T. Nicklee, D. W. Hedley, Effects of the epidermal growth factor receptor inhibitor OSI-774, Tarceva, on downstream signaling pathways and apoptosis in human pancreatic adenocarcinoma. *Mol. Cancer Ther.* **1**, 777–783 (2002).
5. M. J. Moore *et al.*; National Cancer Institute of Canada Clinical Trials Group, Erlotinib plus gemcitabine compared with gemcitabine alone in patients with advanced pancreatic cancer: A phase III trial of the National Cancer Institute of Canada Clinical Trials Group. *J. Clin. Oncol.* **25**, 1960–1966 (2007).
6. D. V. Catenacci *et al.*, Randomized phase Ib/II study of gemcitabine plus placebo or vismodegib, a hedgehog pathway inhibitor, in patients with metastatic pancreatic cancer. *J. Clin. Oncol.* **33**, 4284–4292 (2015).
7. H. L. Kindler *et al.*, Gemcitabine plus bevacizumab compared with gemcitabine plus placebo in patients with advanced pancreatic cancer: Phase III trial of the Cancer and Leukemia Group B (CALGB 80303). *J. Clin. Oncol.* **28**, 3617–3622 (2010).
8. H. L. Kindler *et al.*, Axitinib plus gemcitabine versus placebo plus gemcitabine in patients with advanced pancreatic adenocarcinoma: A double-blind randomised phase 3 study. *Lancet Oncol.* **12**, 256–262 (2011).
9. M. A. Morgan *et al.*, The combination of epidermal growth factor receptor inhibitors with gemcitabine and radiation in pancreatic cancer. *Clin. Cancer Res.* **14**, 5142–5149 (2008).
10. K. P. Olive *et al.*, Inhibition of Hedgehog signaling enhances delivery of chemotherapy in a mouse model of pancreatic cancer. *Science* **324**, 1457–1461 (2009).
11. C. J. Bruns *et al.*, Effect of the vascular endothelial growth factor receptor-2 antibody DC101 plus gemcitabine on growth, metastasis and angiogenesis of human pancreatic cancer growing orthotopically in nude mice. *Int. J. Cancer* **102**, 101–108 (2002).
12. S. Shin, C. M. Park, H. Kwon, K. H. Lee, Erlotinib plus gemcitabine versus gemcitabine for pancreatic cancer: Real-world analysis of Korean national database. *BMC Cancer* **16**, 443 (2016).
13. C. Zheng, X. Jiao, Y. Jiang, S. Sun, ERK1/2 activity contributes to gemcitabine resistance in pancreatic cancer cells. *J. Int. Med. Res.* **41**, 300–306 (2013).
14. X. Jin *et al.*, Fructose-1,6-bisphosphatase inhibits ERK activation and bypasses gemcitabine resistance in pancreatic cancer by blocking IQGAP1-MAPK interaction. *Cancer Res.* **77**, 4328–4341 (2017).
15. Y. X. Zhu *et al.*, LLGL1 regulates gemcitabine resistance by modulating the ERK-SP1-OSMR pathway in pancreatic ductal adenocarcinoma. *Cell. Mol. Gastroenterol. Hepatol.* **10**, 811–828 (2020).
16. Y. H. Su *et al.*, ERK-mediated transcriptional activation of Dicer is involved in gemcitabine resistance of pancreatic cancer. *J. Cell. Physiol.* **236**, 4420–4434 (2021).
17. L. Kraj *et al.*, Calcium channel blockers use and overall survival in pancreatic cancer patients receiving gemcitabine. *J. Clin. Oncol.* **35**, e15756 (2017).
18. U. Ben-David *et al.*, Genetic and transcriptional evolution alters cancer cell line drug response. *Nature* **560**, 325–330 (2018).
19. A. F. Aissa *et al.*, Single-cell transcriptional changes associated with drug tolerance and response to combination therapies in cancer. *Nat. Commun.* **12**, 1628 (2021).
20. D. R. Principe *et al.*, Long-term gemcitabine treatment reshapes the pancreatic tumor microenvironment and sensitizes murine carcinoma to combination immunotherapy. *Cancer Res.* **80**, 3101–3115 (2020).
21. X. Jiang, Y. D. Seo, K. M. Sullivan, V. G. Pillarisetty, Establishment of slice cultures as a tool to study the cancer immune microenvironment. *Methods Mol. Biol.* **1884**, 283–295 (2019).
22. C. Y. Lim *et al.*, Organotypic slice cultures of pancreatic ductal adenocarcinoma preserve the tumor microenvironment and provide a platform for drug response. *Pancreatology* **18**, 913–927 (2018).
23. T. Pantsar, The current understanding of KRAS protein structure and dynamics. *Comput. Struct. Biotechnol. J.* **18**, 189–198 (2019).
24. R. G. McKeever, R. J. Hamilton, "Calcium channel blockers" in *StatPearls* (StatPearls Publishing, Treasure Island, FL, 2021).
25. S. R. Hingorani *et al.*, Trp53R172H and KrasG12D cooperate to promote chromosomal instability and widely metastatic pancreatic ductal adenocarcinoma in mice. *Cancer Cell* **7**, 469–483 (2005).
26. P. A. Philip *et al.*, Phase III study comparing gemcitabine plus cetuximab versus gemcitabine in patients with advanced pancreatic adenocarcinoma: Southwest Oncology Group-directed intergroup trial S0205. *J. Clin. Oncol.* **28**, 3605–3610 (2010).
27. Y. Jia *et al.*, The role of GLI-SOX2 signaling axis for gemcitabine resistance in pancreatic cancer. *Oncogene* **38**, 1764–1777 (2019).
28. Y. Li *et al.*, Natural compound oblongifolin C confers gemcitabine resistance in pancreatic cancer by downregulating Src/MAPK/ERK pathways. *Cell Death Dis.* **9**, 538 (2018).
29. R. Nussinov *et al.*, The key role of calmodulin in KRAS-driven adenocarcinomas. *Mol. Cancer Res.* **13**, 1265–1273 (2015).
30. C. Agamasu *et al.*, KRAS prenylation is required for bivalent binding with calmodulin in a nucleotide-independent manner. *Biophys. J.* **116**, 1049–1063 (2019).
31. M. Fivaz, T. Meyer, Reversible intracellular translocation of KRas but not HRas in hippocampal neurons regulated by Ca^{2+}/calmodulin. *J. Cell Biol.* **170**, 429–441 (2005).
32. B. Sperlich, S. Kapoor, H. Waldmann, R. Winter, K. Weise, Regulation of K-Ras4B membrane binding by calmodulin. *Biophys. J.* **111**, 113–122 (2016).
33. M. Zhang, H. Jang, V. Gaponenko, R. Nussinov, Phosphorylated calmodulin promotes PI3K activation by binding to the SH_2 domains. *Biophys. J.* **113**, 1956–1967 (2017).
34. R. Nussinov, M. Zhang, C. J. Tsai, H. Jang, Calmodulin and IQGAP1 activation of PI3Kα and Akt in KRAS, HRAS and NRAS-driven cancers. *Biochim. Biophys. Acta Mol. Basis Dis.* **1864**, 2304–2314 (2018).
35. M. Zhang *et al.*, Ca^{2+}-dependent switch of calmodulin interaction mode with tandem IQ motifs in the scaffolding protein IQGAP1. *Biochemistry* **58**, 4903–4911 (2019).
36. H. Jang *et al.*, The structural basis of the farnesylated and methylated KRas4B interaction with calmodulin. *Structure* **27**, 1647–1659.e4 (2019).
37. R. Nussinov *et al.*, Calmodulin and PI3K signaling in *KRAS* cancers. *Trends Cancer* **3**, 214–224 (2017).
38. P. Villalonga *et al.*, Calmodulin binds to K-Ras, but not to H- or N-Ras, and modulates its downstream signaling. *Mol. Cell. Biol.* **21**, 7345–7354 (2001).
39. B. Alvarez-Moya, C. López-Alcalá, M. Drosten, O. Bachs, N. Agell, K-Ras4B phosphorylation at Ser181 is inhibited by calmodulin and modulates K-Ras activity and function. *Oncogene* **29**, 5911–5922 (2010).
40. M. Bosch, J. Gil, O. Bachs, N. Agell, Calmodulin inhibitor W13 induces sustained activation of ERK2 and expression of p21(cip1). *J. Biol. Chem.* **273**, 22145–22150 (1998).
41. S. A. Lee *et al.*, Calmodulin-dependent activation of p38 and p42/44 mitogen-activated protein kinases contributes to c-fos expression by calcium in PC12 cells: Modulation by nitric oxide. *Brain Res. Mol. Brain Res.* **75**, 16–24 (2000).
42. M. Illario *et al.*, Calcium/calmodulin-dependent protein kinase II binds to Raf-1 and modulates integrin-stimulated ERK activation. *J. Biol. Chem.* **278**, 45101–45108 (2003).
43. J. M. Schmitt, G. A. Wayman, N. Nozaki, T. R. Soderling, Calcium activation of ERK mediated by calmodulin kinase I. *J. Biol. Chem.* **279**, 24064–24072 (2004).
44. S. Parvathaneni, Z. Li, D. B. Sacks, Calmodulin influences MAPK signaling by binding KSR1. *J. Biol. Chem.* **296**, 100577 (2021).
45. O. Melien *et al.*, Ca^{2+}-mediated activation of ERK in hepatocytes by norepinephrine and prostaglandin F2 alpha: Role of calmodulin and Src kinases. *BMC Cell Biol.* **3**, 5 (2002).
46. K. Yuan *et al.*, Calmodulin mediates Fas-induced FADD-independent survival signaling in pancreatic cancer cells via activation of Src-extracellular signal-regulated kinase (ERK). *J. Biol. Chem.* **286**, 24776–24784 (2011).
47. W. E. Criss, S. Kakiuchi, Calcium: Calmodulin and cancer. *Fed. Proc.* **41**, 2289–2291 (1982).
48. W. N. Hait, J. S. Lazo, Calmodulin: A potential target for cancer chemotherapeutic agents. *J. Clin. Oncol.* **4**, 994–1012 (1986).
49. K. Yuan *et al.*, Calmodulin antagonists promote TRA-8 therapy of resistant pancreatic cancer. *Oncotarget* **6**, 25308–25319 (2015).
50. A. Villalobo, M. W. Berchtold, The role of calmodulin in tumor cell migration, invasiveness, and metastasis. *Int. J. Mol. Sci.* **21**, 765 (2020).
51. S. J. Tingle, G. R. Severs, J. A. G. Moir, S. A. White, Calcium channel blockers in pancreatic cancer: Increased overall survival in a retrospective cohort study. *Anticancer Drugs* **31**, 737–741 (2020).
52. L. Y. Chiu *et al.*, L-type calcium channel blockers reverse docetaxel and vincristine-induced multidrug resistance independent of ABCB1 expression in human lung cancer cell lines. *Toxicol. Lett.* **192**, 408–418 (2010).
53. B. S. Wong, L. Y. Chiu, D. G. Tu, G. T. Sheu, T. T. Chan, Anticancer effects of antihypertensive L-type calcium channel blockers on chemoresistant lung cancer cells via autophagy and apoptosis. *Cancer Manag. Res.* **12**, 1913–1927 (2020).
54. N. Kanwar *et al.*, Amplification of a calcium channel subunit CACNG4 increases breast cancer metastasis. *EBioMedicine* **52**, 102646 (2020).
55. A. Shiozaki *et al.*, Amlodipine and verapamil, voltage-gated Ca^{2+} channel inhibitors, suppressed the growth of gastric cancer stem cells. *Ann. Surg. Oncol.* **28**, 5400–5411 (2021).
56. P. Panneerpandian, D. B. Rao, K. Ganesan, Calcium channel blockers lercanidipine and amlodipine inhibit YY1/ERK/TGF-β mediated transcription and sensitize the gastric cancer cells to doxorubicin. *Toxicol. In Vitro* **74**, 105152 (2021).
57. N. Woods *et al.*, Fendiline inhibits proliferation and invasion of pancreatic cancer cells by interfering with ADAM10 activation and β-catenin signaling. *Oncotarget* **6**, 35931–35948 (2015).
58. H. Jäger *et al.*, Blockage of intermediate-conductance Ca^{2+}-activated K^+ channels inhibit human pancreatic cancer cell growth in vitro. *Mol. Pharmacol.* **65**, 630–638 (2004).
59. D. van der Hoeven *et al.*, Fendiline inhibits K-Ras plasma membrane localization and blocks K-Ras signal transmission. *Mol. Cell. Biol.* **33**, 237–251 (2013).
60. D. R. Principe *et al.*, XP-524 is a dual-BET/EP300 inhibitor that represses oncogenic KRAS and potentiates immune checkpoint inhibition in pancreatic cancer. *Proc. Natl. Acad. Sci. U.S.A.* **119**, e2116764119 (2022).
61. D. R. Principe *et al.*, TGFβ blockade augments PD-1 inhibition to promote T-cell-mediated regression of pancreatic cancer. *Mol. Cancer Ther.* **18**, 613–620 (2019).
62. D. R. Principe *et al.*, Loss of SMAD4 is associated with poor tumor immunogenicity and reduced PD-L1 expression in pancreatic cancer. *Front. Oncol.* **12**, 806963 (2022).